Short Communication:

Enhancement of the Silicon Nanocrystals' Electronic Structure within a Silicon Carbide Matrix

Soni Prayogi[1,2*]

[1]*Department of Electrical Engineering, Pertamina University, Jl. Teuku Nyak Arief, Jakarta 12220, Indonesia*

[2]*Electronics Research Center, National Innovation Research Agency, Jl. M.H. Thamrin No. 8, Jakarta 10340, Indonesia*

* ***Corresponding author:***

email: prayogi.sp@gmail.com

Received: December 7, 2022
Accepted: July 6, 2023

DOI: 10.22146/ijc.79864

Abstract: *Using plasma-enhanced chemical vapor deposition (PECVD), a mixed gas of silane (SiH_4) and methane (CH_4) was diluted with hydrogen (H_2) to produce thin films of silicon nanocrystals embedded in a silicon carbide (SiC) matrix. This method prevents the co-deposition of SiH and SiC from high-temperature annealing procedures. This study experimentally explores the improvement of the electronic structure by adjusting two processing parameters according to classical nucleation theory (ratio of SiH_4 to CH_4 and working gas pressure). The deposited films were examined using ellipsometry spectroscopy, X-ray diffraction, scanning electron microscopy, atomic force microscopy, and photoluminescence to determine grain size, crystal volume fraction, topography, and bond configurations. The results show that increasing the working gas pressure can increase the density of SiC, while increasing the ratio of SiH_4 to CH_4 can only produce larger grain sizes. This is consistent with how SiC works and grows. Without using a high-temperature annealing procedure, this technique can improve the electrical structure of SiC contained in the SiC matrix formed by PECVD.*

Keywords: *methane; silane; hydrogen; silicon carbide; PECVD*

■ INTRODUCTION

Since silicon emits light poorly due to its indirect bandgap, Si-based materials have been investigated ever since the emission from porous silicon was discovered in 1990 [1]. Due to its prospective uses in optoelectronics and photovoltaics [2], silicon carbide (SiC) embedded in a dielectric matrix has recently gained a lot of interest [3]. SiO_2, Si_3N_4, and SiC are materials used to embed SiC in the dielectric [4]. They have corresponding energy band gaps of 8.9, 4.3, and 2.4 eV, respectively [5]. The lower barrier height of SiC results in better between nearby nanocrystals, carrier mobility [6], and exponentially greater transmission probability [7], which are benefits of SiC [8].

Using a variety of low-temperature deposition techniques, such as magnetron co-sputtering (HWCVD) and plasma-enhanced chemical vapor deposition (PECVD) [9], thin layers of silicon and carbon are often deposited [10]. The deposition of thin films by various CVD at low temperatures is thermodynamically nonequilibrium [11], allowing the production of SiC by PECVD without the need for a high-temperature process [12]. Under the right conditions, silicon and carbon-based radicals can combine to form three-dimensional SiC [13]. They used inductively coupled PECVD to develop SiC thin films produced by a mixture of hydrogen-diluted SiH_4 and CH_4 gas at 200 °C for the substrate [14]. This demonstrates the critical role reactive hydrogen atoms play in encouraging the growth of SiC by lowering the free energy of crystallographic facets and lowering the carbon content by removing surface carbon atoms [15].

Here, a novel approach was presented to generate SiC structures from SiH_4 with CH_4 doped by the PECVD technique and reveal the detailed evolution of the electronic structure in p-type SiC and its relationship to photovoltaic performance (Fig. 1). One crucial aspect of the application of SiC is its electronic structure. The possibility of improving the structure of Si-electrical C

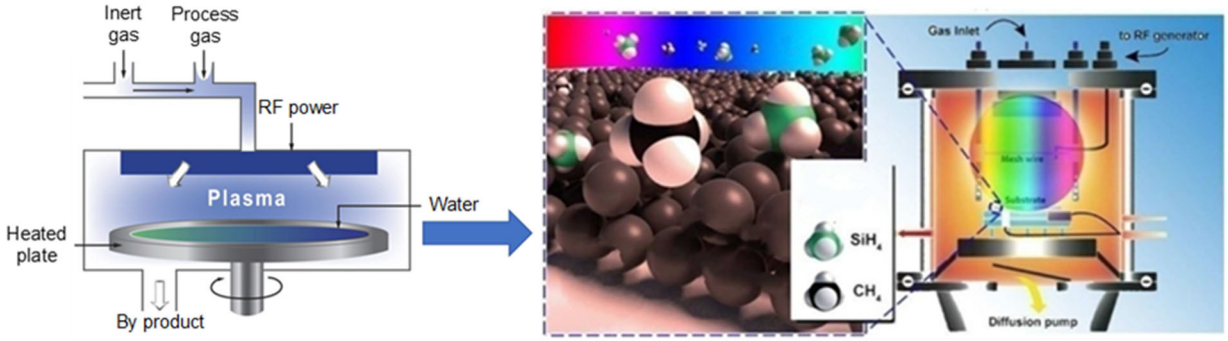

Fig 1. Schematic of PECVD in SiC samples

when thin films of SiC were PECVD-deposited at a low substrate temperature was experimentally investigated in this study. Such as adjusting the SiH_4 to CH_4 ratio, we intended to enhance the nanocrystalline electronic structure by increasing the reactive radical flux.

■ EXPERIMENTAL SECTION

Materials

The process of synthesis of SiC materials involves a chemical reaction between silane gas and carbon at high temperatures. SiC material was grown on Corning glass 7059 substrate which had been prepared with indium tin oxide (ITO) [16]. SiH_4 gas with a concentration of 10% in H_2 was used as the source gas. Furthermore, it is used as a diborane dopant gas with a gas concentration of 10%; in H_2 for the dopant layer, the addition of CH_4 is used as an optimization of the transparent SiC layer and is able to increase the concentration of charge carriers. The growth parameters used are shown in Table 1.

Instrumentation

Using PECVD and a combination of SiH_4 and CH_4 that had been diluted with H_2, SiC was created at a substrate temperature of 270 °C [17]. According to the film deposition, the reactor was emptied to a gas pressure of 1×10^4 Pa by a molecular turbo pump. In order to place the samples on an ITO glass, either the flow ratio of SiH_4 to CH_4 was changed at a constant working gas pressure (P), or P was changed at a constant R. R was set to 5, 10, and 15 among the samples, and the total flow of $SiH_4 + CH_4 + H_2$ was kept constant.

The crystalline properties were evaluated by grazing incidence XRD with SHIMADZU at 40 kV, 40 mA, and Cu Kα radiation (λ = 1.54 Å). The Scherrer equation determines the nanocrystal size. Spectroscopy ellipsometry (V-Vase) is used to examine other electronic structure characteristics, such as crystallinity and phase characteristics. Spectroscopy ellipsometry and XRD spectra allowed for the detection of grains and crystal volume fractions. Spectroscopy ellipsometry was used to identify the silicon, carbon, and hydrogen bond configurations. In this work, spectroscopy ellipsometry with a visible range of 0.5 to 6.5 eV was employed. SEM (Hitachi S-4800) and AFM (Park NX10) were used to examine the topography. The constant and time-resolved Photoluminescence (PL) spectra were acquired using a HORIBA Jobin Yvon FM-4P-TCSPC spectrophotometer with a 300 nm excitation and a 460 nm probe.

Table 1. Parameters for the deposition of SiC

Deposition parameters*	p-Type layer of amorphous silicon carbon (a-SiC: H)		
	R-5	R-10	R-15
Flow rate SiH_4 (sccm)	20	20	20
Flow rate B_2H_6 (sccm)	2	2	2
Flow rate H_2 (sccm)	20	20	20
Flow rate CH_4 (sccm)	10	20	30

*Power RF = 5 Watt, temperature = 210 °C, pressure = 4800 mTorr, time = 10 min

Procedure

The process of synthesis of SiC materials using PECVD involves a chemical reaction catalyzed by plasma at low pressure to produce a thin layer of SiC. The following are the stages of the process. Substrate Preparation: Before the process begins, the substrate that will be deposited with a SiC layer must be properly prepared. The substrate is usually made of a material such as glass, silicon, or metal suitable for supporting the SiC layer. Precursor Filling: The precursor is a chemical gas containing the elements required to form SiC. In the PECVD process, the precursors used contain silicon and carbon. Usually, SiH_4 or trichlorosilane ($SiHCl_3$) are used as silicon precursors, while CH_4 or ethylene (C_2H_4) are used as carbon precursors. Production of Plasma: Precursor gases are broken down into radicals by plasma generated by high electrical energy sources. Usually, radio frequency or microwave power is used to form plasma. Plasma allows chemical reactions to occur at lower temperatures than conventional thermal reactions, thereby reducing damage to the substrate. SiC Layer Deposition: Radicals from silicon and carbon precursors react in the plasma and deposit a SiC layer on the surface of the substrate. This process takes place at a low vacuum pressure to ensure that the precursor molecules do not collide with other gases before reaching the substrate. Finishing and Characterization: After the deposition process is complete, the substrate, which has now been covered with a thin layer of SiC, is removed from the reaction chamber. The SiC layer formed will then be tested and characterized to ensure its thickness, crystal structure, hardness, and other properties.

■ RESULTS AND DISCUSSION

The author considers how increasing the R might be possible for SiH_4 to CH_4 to enhance the electronic structure of SiC. The structural characteristics were examined using XRD and spectroscopy ellipsometry techniques, after which the silicon, carbon, and hydrogen bond configurations were covered. Finally, the changing nucleation density was estimated by observing the various surface images produced by SEM and AFM, as well as crystal volume fractions and grain sizes.

The AFM and SEM images of the collection of sample surfaces and cross-sections SiC at R = 5, 10, and 15 are displayed in Fig. 2. The cross-sectional photographs in Fig. 2(a-c) clearly show that the films are fine and that the film–substrate contact is smooth and unobstructed. According to the surface morphology in Fig. 2(d-f), in accordance with the previously mentioned improvement in electronic structure, nanoscale grains uniformly cover the entire substrate [18], and the films grow more compact as the ratio R rises. Fig. 2(d-f) illustrates a general trend of increasing grain size and crystal volume fraction with increasing SiH_4/CH_4 ratio. The decreasing degree is placed inset in the lower right corner and it is known as the relative value of the crystal volume fraction or grain size, referred to as their lowest value in Fig. 3(f). These insets show several growing patterns [19]. However, as observed in Fig. 3(a), the increase in crystal volume fraction is less significant than the increase in grain size when the R of SiH_4 to CH_4 rises, showing that the electronic structure is not improved.

The fits from their analysis are displayed in Fig. 3 along with the experimental ψ and Δ data for R-5, R-10, and R-15. We demonstrate the imaginary part of the complicated dielectric functions obtained using the spectroscopy ellipsometry at room temperature in the optical energy range of 0.6–6.6 eV in Fig. 4(a) to support the development of the excitation [20]. Fig. 4(a) for R-5 sample shows two different exciton peaks, E-1 = 1.04 eV and E-2 = 4.64 eV, with a large energy shift between them of 3.60 eV. These measurements were made on SiC using spectroscopy ellipsometry. Furthermore, it's crucial to note that the SiC film lacks the spectral weight transfer that is visible in the R-5 film at $<\varepsilon_2>$. It turns out that the SiC film's peak in $<\varepsilon_2>$ occurs at high energy, specifically at E-2 = 5.34 eV. A typical signature of electronic correlation is a transfer of spectral weight of 3 eV from higher energy to lower energy at E-1, which is present at 3.32 eV. Fig. 4(a) shows the R-10 sample $<\varepsilon_2>$ curve, which highlights both the quantum confinement effect and the tremendous impact of hydrogen carbon [21]. Both exciton peaks are observed to shift toward one another and merge into the exciton R-15. In the case of the R-15 sample, when more H_2 is introduced in Fig. 4(a),

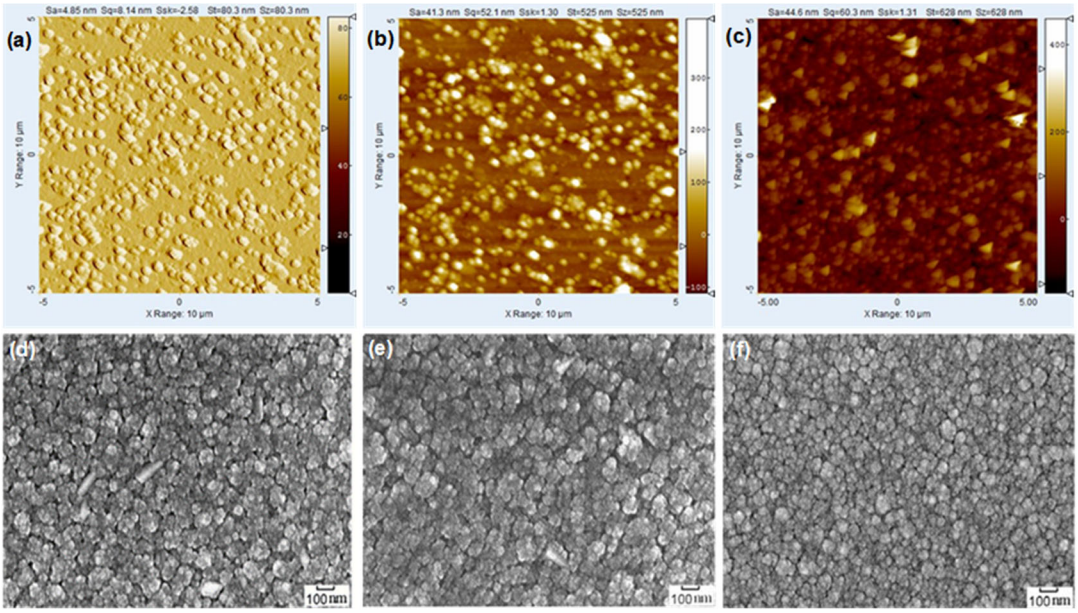

Fig 2. Morphology and structure of SiC measured by AFM with dimensions of 10×10 μm^2 for (a) R-5, (b) R-10, and (c) R-15. Surface and cross-sectional SEM images of SiC (d) R-5, (e) R-10, and (f) R-15

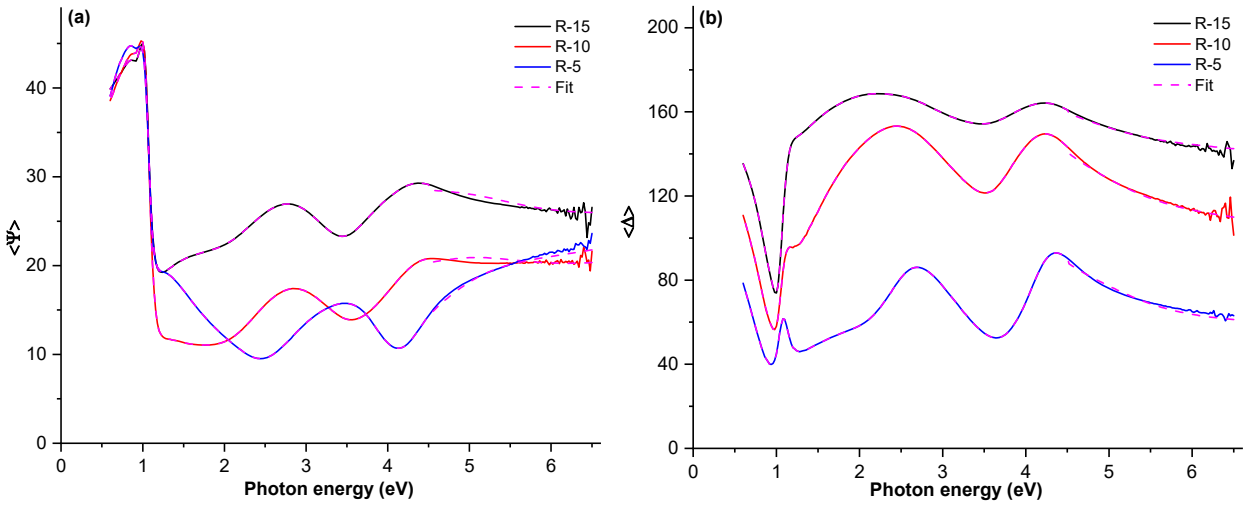

Fig 3. The parameters of spectroscopic ellipsometry (a) ψ and (b) **Δ** for the SiC layers

the <ε$_2$> curve between E-1 = 1.02 eV and E-2 = 4.36 eV shifts by a further 3.34 eV. This results in a revolving excitement characteristic that is like that of the SiC film [22]. This indicates that the electrical structure of the SiC film that was formed has been significantly tuned by the hydrogen carbon.

The nano-structural characteristics of films have been deposited using XRD. The SiC samples' XRD spectra are shown in Fig. 4(b). To determine the degree of crystallinity of films as they are being deposited, in order to account for the film thickness, we first normalize. The diffraction peak for the first set of samples SiC is only visible at 2 = 28.4°, as shown in Fig. 4(b), and it originates from the silicon's (111) crystal planes. These peaks are attributable to the silicon crystal planes (220) and (311), respectively. According to these samples of SiC, if we raise R, the preferred diffraction progressively peaks at (111) and gets more intense while the maximum complete widths steadily decrease, showing an improvement in grain size, and further increases in crystallinity [23]. No diffraction

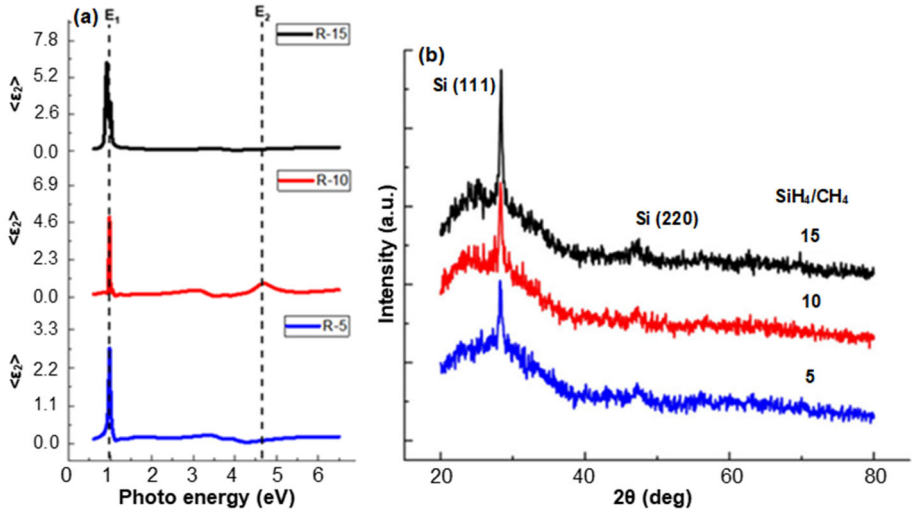

Fig 4. (a) Dialectic function <ε_2> and (b) XRD data for SiC structure deposited at different flow ratios of SiH_4/CH_4

peaks are associated with crystalline SiC or crystalline carbons [24]. The films of the hydrogenated SiC alloy were examined employing the radio frequency PECVD for the phase change of silicon from microcrystalline to nanocrystalline [25]. The XRD spectrum was used to calculate the grain sizes.

The PL SiC attenuation in Fig. 5(a) shows SiC in the same time range, showing almost the same for all samples R-5, R-10, and R-15. However, when viewed the transient photocurrent response of SiC in Fig. 5(b) also shows a clearly larger value in the R-15 sample compared to the other samples. All these findings conclusively demonstrate the enhancement of SiC electron transport, which undoubtedly aids in the enhanced photocatalytic CH_4 reduction [26]. This was thought that when SiH_4 was used as a co-catalyst in photocatalytic CH_4 reduction, the generated CH_4, even in small amounts, would form stable chemical adsorption with SiC and therefore block the active sites.

Based on the experimental findings, Fig. 6 schematically depicts a potential pathway for selecting SiH_4 to CH_4 over SiC. As a result of the high energy barrier that had to be overcome, charge transfer from the excited state of the electron donor served as the driving force for the hydrogenation of SiH_4. While the CH_4 served

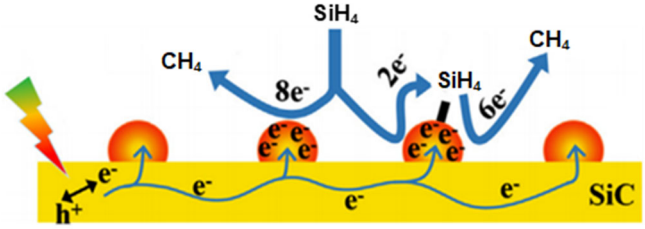

Fig 6. The deep photoreduction of SiH_4 and CH_4 to SiC is depicted schematically using a likely

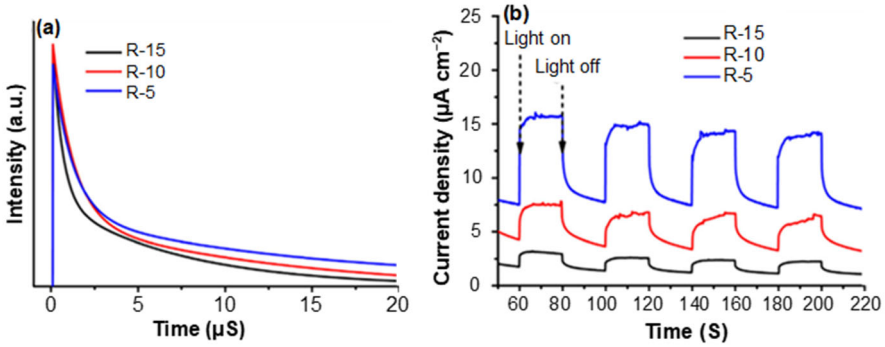

Fig 5. (a) PL spectroscopy stimulated by incoming light of 300 nm over time and (b) the current SiC photocurrent measurements

as both the electron trapping agent and the active sites in the SiH_4 reduction reaction in our case of SiC, the ultrathin SiC chose to supply energetic electrons with substantial reduction potential [27]. The deep reduction of SiH_4 to produce CH_4 was therefore encouraged by the SiC, which not only decreased the risk of SiH_4 poisoning on SiC but also increased the efficiency of CH_4 generation.

The structural analyses of as-deposited SiC reveal that raising working gas pressure while maintaining a fixed ratio of SiH_4 to CH_4 can increase SiC electronic structure, which is in accordance with the previously mentioned theory of nucleation [28]. The experimental findings show that an increased SiH_4 to CH_4 ratio at a fixed working gas pressure can only result in a rise in grain size but not in electronic structure. This result is inconsistent with the band structure. An understanding of SiC films' electrical structural processes can help with the comprehension of the occurrence [29]. By utilizing gas phase processes, it is possible to explain the experimental findings that show that raising the working gas pressure causes an increase in electronic structure [30]. The working gas pressure increases the likelihood of interactions between the different species. The SiC forms in the gas phase and is then incorporated into the developing films.

■ CONCLUSION

In summary, PECVD at a low substrate temperature of 270 °C has been used to develop SiC films made from a combination of SiH_4, CH_4, and H_2. The prospect of raising the electronic structure is studied by the reactant gases SiH_4 to CH_4 ratio being increased. The experimental findings showed that raising the SiH_4 to CH_4 ratio is likely to be sole. Highly hydrogenated developing surfaces have lower surface diffusion energies and a larger surface capacity to diffuse radical absorption, according to the examination of the silicon nanocrystal nucleation mechanism. As the flux of precursor impinging on it rises, the radical absorption on the increasing surface is simply incorporated into the silicon nucleus rather than forming a new nucleus. However, species interactions in the gas phase can create electronic structures that support the electrical structure of already-deposited films as the overall working pressure increases. The method presented in this paper provides a practical way of increasing the density of SiC embedded in SiC produced by PECVD without using a high-temperature technique.

■ ACKNOWLEDGMENTS

The authors thank the Ministry of Education and Culture of the Republic of Indonesia for their support in providing Indonesian and Research Scholarships (179/E5/PG.02.00/PL/2023) and jobs at Pertamina University (093/UP-WRP.1/PJN/VII/2023 and 0044/UP-R/SK/HK.01/II/2023). The author would like to thank the ITS Research Center and Singapore Synchrotron Light Source (SSLS) for providing the facilities needed to conduct research. SSLS is the National Research Infrastructure under the National Research Foundation Singapore.

■ REFERENCES

[1] Meng, F., Shen, L., Shi, J., Zhang, L., Liu, J, Liu, Y., and Liu, Z., 2015, Role of the buffer at the interface of intrinsic a-Si:H and p-type a-Si:H on amorphous/crystalline silicon heterojunction solar cells, *Appl. Phys. Lett.*, 107, 223901.

[2] Zahoor, R., Jalil, A., Ilyas, S.Z., Ahmed, S., and Hassan, A., 2021, Optoelectronic and solar cell applications of ZnO nanostructures, *Results Surf. Interfaces*, 2, 100003.

[3] Baskar, S., and Pratibha, N.R., 2016, Synthesis and characterization of silicon nanocrystals in SiC matrix using sputtering and PECVD techniques, *Mater. Today: Proc.*, 3 (6), 2121–2131.

[4] Lükermann, F., Heinzmann, U., and Stiebig, H., 2012, Plasmon enhanced resonant defect absorption in thin a-Si:H n-i-p devices, *Appl. Phys. Lett.*, 100 (25), 253907.

[5] Wen, X., Chen, C., Lu, S., Li, K., Kondrotas, R., Zhao, Y., Chen, W., Gao, L., Wang, C., Zhang, J., Niu, G., and Tang, J., 2018, Vapor transport deposition of antimony selenide thin film solar cells with 7.6% efficiency, *Nat. Commun.*, 9 (1), 2179.

[6] Huang, X., Wu, Q., Dai, R., Ning, J., Zhang, L., Wang, W., Xue, S., Yan, J., Zhang, F., and Zhang, W., 2022, A density functional study of the

structural, electronic, optical and lattice dynamical properties of $AgGaS_2$, *Results Phys.*, 35, 105309.

[7] Kim, J., Hong, Z., Li, G., Song, T., Chey, J., Lee, Y.S., You, J., Chen, C.C., Sadana, D.K., and Yang, Y., 2015, 10.5% efficient polymer and amorphous silicon hybrid tandem photovoltaic cell, *Nat Commun.*, 6 (1), 6391.

[8] Pandey, A., Bhattacharya, S., Panigrahi, J., Mandal, S., and Komarala, V.K., 2022, Effect of gas flow rate in PECVD of amorphous silicon thin films for interface passivation of silicon heterojunction solar cells, *Phys. Status Solidi A*, 219 (16), 2200183.

[9] Prayogi, S., Cahyono, Y., and Darminto, D., 2022, Electronic structure analysis of a-Si:H p-i1-i2-n solar cells using ellipsometry spectroscopy, *Opt. Quantum Electron.*, 54 (1), 732.

[10] Prayogi, S., Ayunis, A., Kresna, K., Cahyono, Y., Akidah, A., and Darminto, D., 2017, Analysis of thin layer optical properties of A-Si:H p-type doping CH_4 and p-type without CH_4 is deposited PECVD systems, *J. Phys.: Conf. Ser.*, 853 (1), 012032.

[11] Beake, B.D., McMaster, S.J., and Liskiewicz, T.W., 2022, Contact size effects on the friction and wear of amorphous carbon films, *Appl. Surf. Sci. Adv.*, 9, 100248.

[12] Joo, K.N., and Park, H.M., 2022, Recent progress on optical tomographic technology for measurements and inspections of film structures, *Micromachines*, 13 (7), 1074.

[13] Buriak, J.M., and Sikder, M.D.H., 2015, From molecules to surfaces: Radical-based mechanisms of Si–S and Si–Se bond formation on silicon, *J. Am. Chem. Soc.*, 137 (3), 9730–9738.

[14] Prayogi, S., Asih, R., Priyanto, B., Baqiya, M.A., Naradipa, M.A., Cahyono, Y., Darminto, D., and Rusydi, A., 2022, Observation of resonant exciton and correlated plasmon yielding correlated plexciton in amorphous silicon with various hydrogen content, *Sci. Rep.*, 12 (1), 21497.

[15] Yokosuk, M.O., Tiwald, T.E., Saunders, D.L., Blake, T.A., and Myers, T.L., 2021, Combining spectroscopic techniques to determine the optical constants of powdered lactose, *Appl. Opt.*, 60 (8), 2412–2421.

[16] Prayogi, S., Cahyono, Y., Hamdani, D., and Darminto, D., 2022, Effect of active layer thickness on the performance of amorphous hydrogenated silicon solar cells, *Eng. Appl. Sci. Res.*, 49 (2), 201–208.

[17] Prayogi, S., Cahyono, Y., Iqballudin, I., Stchakovsky, M., and Darminto, D., 2021, The effect of adding an active layer to the structure of a-Si: H solar cells on the efficiency using RF-PECVD, *J. Mater. Sci.: Mater. Electron.*, 32 (6), 7609–7618.

[18] Abubakar, S., Ying Chyi, J.L., Tan, S.T., Sagadevan, S., Talib, Z.A., and Paiman, S., 2021, Nanoscale domain imaging and the electromechanical response of zinc oxide nanorod arrays synthesized on different substrates, *J. Mater. Res. Technol.*, 14, 2451–2463.

[19] Bakonyi, I., 2021, Accounting for the resistivity contribution of grain boundaries in metals: Critical analysis of reported experimental and theoretical data for Ni and Cu, *Eur. Phys. J. Plus*, 136 (4), 410.

[20] Santoso, I., Gogoi, P.K., Su, H.B., Huang, H., Lu, Y., Qi, D., Chen, W., Majidi, M.A., Feng, Y.P., Wee, A.T.S., Loh, K.P., Venkatesan, T., Saichu, R.P., Goos, A., Kotlov, A., Rübhausen, M., and Rusydi, A., 2011, Observation of room-temperature high-energy resonant excitonic effects in graphene, *Phys. Rev. B*, 84 (8), 081403.

[21] Yeo, L.H., Srivastava, A., Majidi, M.A., Sutarto, R., He, F., Poh, S.M., Diao, C., Yu, X., Motapothula, M., Saha, S., Ojha, S., Kanjilal, D., Trevisanutto, P.E., Breese, M.B.H., Venkatesan, T., and Rusydi, A., 2015, Anomalous spectral-weight transfers unraveling oxygen screening and electronic correlations in the insulator-metal transition of VO_2, *Phys. Rev. B*, 91 (8), 081112.

[22] Ren, N., Zhu, J., Shi, P., Shan, Q., Li, T., Wei, C., Zhao, Y. and Zhang, X., 2018, Controlling performance of a-Si:H solar cell with SnO_2:F front electrode by introducing dual p-layers with p-a-SiO_x:H/p-nc-SiO_x:H nanostructure, *Sol. Energy*, 171, 907–913.

[23] Forouhi, A.R., and Bloomer, I., 2019, New dispersion equations for insulators and semiconductors valid throughout radio-waves to extreme ultraviolet spectral range, *J. Phys. Commun.*, 3 (3), 035022.

[24] Bohórquez, C., Bakkali, H., Delgado, J.J., Blanco, E., Herrera, M., and Domínguez, M., 2022, Spectroscopic ellipsometry study on tuning the electrical and optical properties of Zr-doped ZnO thin films grown by atomic layer deposition, *ACS Appl. Electron. Mater.*, 4 (3), 925–935.

[25] Chakraborty, M., Banerjee, A., and Das, D., 2014, Spectroscopic studies on nanocrystalline silicon thin films prepared from H_2-diluted SiH_4-plasma in inductively coupled low pressure RF PECVD, *Phys. E*, 61, 95–100.

[26] Mateo, D., Cerrillo, J.L., Durini, S., and Gascon, J., 2021, Fundamentals and applications of photo-thermal catalysis, *Chem. Soc. Rev.*, 50 (3), 2173–2210.

[27] Mortelliti, M.J., Wang, A.N., and Dempsey, J.L., 2021, Interfacial electron transfer through ultrathin ALD TiO_x layers: A comparative study of TiO_2/TiO_x and SnO_2/TiO_x core/shell nanocrystals, *J. Phys. Chem. C*, 125 (23), 12937–12959.

[28] Prayogi, S., Cahyono, Y., and Darminto, D., 2021, Fabrication of solar cells based on a-Si: H layer of intrinsic double (P-i_x-i_y-N) with PECVD and efficiency analysis, *J. Phys.: Conf. Ser.*, 1951 (1), 012015.

[29] Gueye, M.N., Carella, A., Faure-Vincent, J., Demadrille, R., and Simonato, J.P., 2020, Progress in understanding structure and transport properties of PEDOT-based materials: A critical review, *Prog. Mater. Sci.*, 108, 100616.

[30] le Saché, E., and Reina, T.R., 2022, Analysis of dry reforming as direct route for gas phase CO_2 conversion. The past, the present and future of catalytic DRM technologies, *Prog. Energy Combust. Sci.*, 89, 100970.